LAWRENCE
LIVERMORE
NATIONAL
LABORATORY

UCRL-CONF-212233

Fracture Permeability Evolution in Desert Peak Quartz Monzonite

S. R. Carlson, J. J. Roberts, R. L. Detwiler, B. E. Viani, S. K. Roberts

May 12, 2005

Geothermal Resources Council
Reno, NV, United States
September 25, 2005 through September 28, 2005

UCRL-CONF-212233

Fracture Permeability Evolution in Desert Peak Quartz Monzonite

Steven R. Carlson, Jeffery J. Roberts, Russell L. Detwiler, Brian E. Viani, and Sarah K. Roberts

Lawrence Livermore National Laboratory
Livermore, California 94551

Key words: fracture permeability, fluid-rock interactions, flow simulations, surface profilometry, resistivity, Desert Peak, EGS

Abstract

Fracture flow experiments are being conducted on quartz monzonite core from the Desert Peak East EGS site, Churchill County, Nevada. The flow experiments are conducted at temperatures of 167-169°C and 5.5 MPa confining pressure through artificial fractures. Two injection fluids, a saline solution and a silica-bearing solution, have been used to date. Flow rates are typically 0.02 mL/min, but other rates have been used. The fracture surfaces are characterized with a contact profilometer. The profilometry data demonstrate that it is possible to fabricate statistically similar fracture surfaces and enable us to map aperture variations, which we use in numerical simulations. Effluent samples are collected for chemical analysis. The fluid pressure gradient is measured across the specimen and effective hydraulic apertures are calculated. The experiments show a reduction in permeability over time for both injection fluids, but a more rapid loss of permeability was observed for the silica-bearing solution. The calculated hydraulic aperture is observed to decrease by 17% for the saline solution and 75% for the silica-bearing fluid, respectively. Electrical resistivity measurements, which are sensitive to the ionic content of the pore fluid, provide additional evidence of fluid-rock interactions.

Introduction

The Desert Peak East EGS Project is an industry-DOE sponsored effort to investigate the technical feasibility of creating an enhanced geothermal reservoir east of the Desert Peak geothermal field in the Hot Springs Mountains, Churchill County, Nevada (Robertson-Tait and Morris, 2003). The performance of an enhanced geothermal system depends on both the ability to create new fractures and the ability to maintain fracture permeability over time. Physical and chemical processes that may diminish fracture permeability include pressure-enhanced dissolution at asperities and the precipitation of silica and other minerals in flow channels. Our goal is to identify the physical and chemical effects that alter fracture permeability in Desert Peak quartz monzonite.

Several previous studies have examined fluid flow through crushed granite at geothermal temperatures. Chigira and Watanabe (1994) studied silica precipitation in granite powder under a negative temperature gradient, and Plagnes *et al*. (2000) studied the effect of fluid salinity on mineral dissolution rates. Other studies have documented the dissolution of various minerals, including calcite, quartz, biotite, potassium feldspar and plagioclase,

during fluid flow through granite at elevated temperatures (*e.g.*, Moore *et al.*, 1983; Savage *et al*., 1992; Azaroual and Fouillac, 1997).

Moore *et al*. (1994) observed reductions in permeability during extended flow experiments through intact specimens of Westerly granite at 50 MPa effective pressure and temperatures between 300° and 500°C. Morrow *et al*. (2001) have since extended this work to lower temperatures (150°C) and to fractured specimens. In their experiments, pore fluids were cycled back and forth through the sample and the observed reductions in permeability were attributed to fracture sealing by mineral growth and precipitation. Polak *et al*. (2003) and Yashara and Elsworth (2004) studied fracture permeability reduction in novaculite at temperatures to 150°C and 3.5 MPa effective pressure. They attributed approximately 80% of the observed reduction in fracture aperture to pressure solution.

Carlson *et al.* (2004) reported results from initial experiments in which a saline solution was flowed through Desert Peak quartz monzonite. A reduction in fracture permeability was seen in one specimen, along with indirect evidence of mineral dissolution from electrical resistivity data. New flow experiments using a silica-bearing fluid, combined with measurements of fracture topography, the collection of effluent samples and numerical simulations of flow are reported here. Viani *et al.* (this issue) report in detail on the geochemical modeling of fluid-rock interactions related to these experiments.

Methods

Specimen Preparation

The sample materials are quartz monzonite cores retrieved at a depth of 1210 m from borehole 35-13 TCH. The specimen mineralogy consists of 44% plagioclase, 23% potassium feldspar, 7% quartz and 3% mica (Lutz, 2003). The rock contains numerous, sealed fractures in-filled with secondary minerals such as kaolin (6%), calcite (4%), and dolomite (4%). Sample porosities, calculated from the dry and saturated specimen weights, are about 2%. This value is likely an upper bound on the porosity as the measurements include microcracks induced by cooling and stress release upon retrieval from depth. A more complete geologic description of rock samples from borehole 13-35 TCH is provided by Lutz *et al.* (2003).

Flow measurements are made through artificial fractures cut along the long axis of each core. One saw-cut surface is bead blasted and the other is hand lapped. This technique has several advantages: the fracture surfaces have similar and reproducible initial roughness facilitating comparison between different experiments, small geochemical alterations of the non-bead-blasted surface can be detected, and the configuration of each sample is the same, facilitating experimental set-up. A contacting stylus profilometer (Durham and Bonner, 1993) is used to record the topography of the fracture surfaces. The profiling is performed on a rectangular grid of points spaced 200 μm by 200 μm with a vertical resolution of 5 μm. The profiled area is 960 mm^2, greater than 87% of the fracture surface. Apertures are computed by subtracting the measured depths to contact relative to a horizontal baseline.

Pore Fluid Compositions

Two injection fluids have been used to date (Table 1). The saline solution, which was used in the first three experiments, was prepared by adding 8.5 g/L of high-purity NaCl to de-ionized water. The silica solution, used in experiment DP 3972.4, has nearly the same total concentration of dissolved salts, but also contains 58 mg/L of amorphous silica, bringing it close to silica saturation at room temperature and pressure. The silica solution is intended to be more representative of real geothermal fluids, while still remaining comparable to the earlier fluid in pH and electrical conductivity.

Experimental Apparatus

The test specimens are jacketed in Viton tubing and fitted with Hastelloy endcaps. Each endcap contains a narrow reservoir aligned with the fracture. Two perforated platinum disks contact the ends of the cylindrical test specimen and serve as electrodes. Thin mica inserts provide electrical insulation between the endcaps and the mounting frame, which provides a small end load to the sample. A vacuum saturation technique is used to saturate the specimens with one of the pore fluids described above.

Figure 1. Pressure vessel/specimen assembly

The test specimen is inserted into an externally heated, hydrostatic pressure vessel (Figure 1). An APCS syringe pump controls confining pressure at 5.5 MPa. Three Yokogawa temperature controllers maintain confining fluid temperature at 167-169°C. Thermocouples measure confining fluid temperature near the specimen and pore fluid temperature in both endcaps. The inlet pore fluid line is arranged in a loop so that at slow flow rates the upstream fluid attains the same temperature as the rock specimen before entering the fracture. Two Isco 500D syringe pumps control the pore fluid supply. The downstream pump controls pore pressure, at either 1.7 or 2.1 MPa, and the upstream pump controls flow rate, usually 0.02 mL/min, by continually adjusting the inlet reservoir pressure. The pressure drop across the specimen is measured with a Validyne DP 215-50 differential pressure transducer, and other transducers measure the confining and pore fluid pressures. The pressure transducer and thermocouple voltages are read with a digital multimeter, and resistance measurements are made at 1 kHz with an HP 4284 LCR meter. The syringe pumps and the data acquisition system are under computer control. A Harvard Apparatus 22 syringe pump on the downstream pore fluid line allows fluid specimens to be collected without lowering pore pressure. Fluid samples are collected at a rate of 0.02 mL/min so that the fluid residence time remains unchanged. Electrical conductivity of the fluid samples is measured at room temperature with an Omega PHB-70X water analyzer, and pH is measured with an Orion 720A pH meter. Techniques used to determine fluid chemical compositions are described in Viani *et al.* (this issue).

Procedures

Experimental variables are summarized in Table 2. Normally, flow is maintained at a steady rate of 0.02 mL/min. Slower flow rates were also used near the end of experiment DP 3972.1, and on a few occasions, flow has been stopped for up to one week, so that electrical resistance could be monitored under no flow conditions. Brief tests, in which

the flow rate is varied from zero to at most 2.0 mL/min, are made at selected times to measure differential pressure as a function of flow rate. The resulting data are used to calculate effective hydraulic aperture. Experiment DP 3972.3 was intended to observe the effects of thermal stress on fracture permeability by injecting cooler fluid at rapid flow rates. The specimen was subjected to several brief intervals of rapid flow; usually several tens of mL/min, with a maximum flow rate of 167 mL/min. The rapid flow tests were made on selected days; during most of the experiment flow was stopped. In experiment DP 3972.4 flow was maintained at a constant rate of 0.02 mL/min apart from two brief variable flow rate tests.

Results

Fracture Surface Characterization

The initial fracture surface topography was measured for specimens DP 3972.3 and DP 3972.4 with a contacting stylus profilometer and apertures were calculated. A perspective view of the aperture field for specimen DP 3972.4 and a plan view of the bead-blasted surface are shown in Figure 2. The dominant flow direction is from top to bottom. The vertical exaggeration in the perspective view is about 30x. The bead-blasted surface is much rougher than the lapped surface, and so contributes predominately to the aperture field. Because apertures are plotted, the peaks in the perspective view essentially correspond to low points on the bead-blasted fracture surface. Dark areas in the plan view represent highs and light areas are depressions. The specimen contains a number of natural cracks, many of them oriented at a high angle to the specimen axis. One of these can be clearly seen as a white line running from the upper left corner to the right-hand edge. The crack shows up as a "ridge" in the aperture map on the left. If the aperture map is examined closely, one can see that surface topography is fairly anisotropic in this specimen. Aperture "ridges" appear to be preferentially aligned at a high angle to the flow direction, an effect we attribute to small, natural cracks.

Figure 2. Fracture aperture map and bead-blasted surface topography prior to flow

The aperture frequency distributions are approximately log-normal and appear remarkably similar for the two profiled specimens (Figure 3a). With no applied load, the modal aperture is about 0.08 mm, and apertures greater than 0.2 mm are extremely rare. Confining pressure would shift the distributions to the left. Semi-variograms have been calculated both parallel and perpendicular to the dominant flow direction (Figure 3b). They show that the surface topography is uncorrelated at distances greater than 2 or 3 mm in the dominant flow direction. Perpendicular to flow, the correlation persists for as much as 7 or 8 mm, which represents about one-third of the specimen diameter.

Figure 3. Aperture distribution and semi-variograms

Fracture Permeability

We have completed flow experiments on four samples. Effective hydraulic apertures, given in Table 3, were calculated by regressing imposed flow rates against measured pressure gradients Errors were estimated from the standard errors of the linear regression

slopes. Effective hydraulic apertures were measured prior to flow for all but our first specimen, DP 3972.2. An initial hydraulic aperture of 14 μm was found for specimen DP 3972.1. The two more recent specimens, DP 3972.3 and DP 3972.4, have very similar aperture distributions and nearly identical initial hydraulic apertures: 33 and 36 μm, respectively.

Although a large drop in effective hydraulic aperture was observed for specimen DP 3972.1, a jacket leak was discovered at the end of the experiment that calls into question the result, particularly during the late stage of the experiment. Jacket failure occurred in specimen DP 3972.2 after 38 days, and no clear trend was observed in the differential pressure data. The third specimen, DP 3972.3, was subjected to several short episodes of very rapid flow, rather than a prolonged interval of slow constant flow. During the rapid flow episodes, water temperature at the fracture inlet fell as much as 40°C below the reservoir temperature. In addition to thermal perturbations, mechanical flexing of the fracture and surface damage at the asperities may have occurred as the fluid was forced through. Larger pressure gradients were required to push fluid through the fracture at the end of the experiment than at the beginning (Figure 4). The reduction in effective hydraulic aperture for specimen DP 3972.3 is about 17%.

Figure 4. Flow versus pressure gradient for specimen DP 3972.3

The latest experiment, DP 3972.4, used the silica-bearing solution as the injection fluid, and flow was maintained for 37 days at a fixed rate of 0.02 mL/min, except for a few brief interruptions. A nearly continuous, upward trend in differential pore pressure is observed for specimen DP 3972.4 (Figure 5) indicating a reduction in effective hydraulic aperture of over 75%, from 36 to 8 μm (Table 3).

Figure 5. Differential pressure over time for DP 3972.4

At sufficiently slow, constant flow rates, the pressure gradient across the specimen is inversely proportional to permeability by Darcy's law. For flow at 0.02 mL/min, used in experiment DP 3972.4, we calculate a Reynolds number of less than one, indicative of laminar flow. This low Reynolds number and the observed linearity between pressure gradients and flow rates to 2.0 mL/min, indicate that we can reasonably apply Darcy's law. From the specimen geometry, the fluid viscosity, the applied flow rate and measured differential pressures we can calculate permeability for our specimen (Figure 6). The calculated specimen permeabilities are smaller than the fracture permeability because the cross-sectional area of the specimen is much larger than that of the fracture. The calculated permeabilities decline exponentially over time, consistent with earlier flow observations in Westerly granite by Morrow *et al.* (2001).

Figure 6. Permeability for specimen DP 3972.4

Resistivity

The electrical resistance measurements provide indirect evidence of geochemical activity because precipitation and dissolution may change the ionic content of the pore fluid. Temperature and fracture aperture changes also affect electrical resistivity. As we are

able to control temperature to within a few tenths of one degree Celsius, temperature fluctuations may add noise to the resistivity data, but are unlikely to account for long-term trends. In general, we have observed resistivity to rise during constant flow intervals and to fall when flow is stopped. Declines in resistivity during shut-in suggest that ions are dissolving into the pore fluid over time making it more conductive. When flow resumes, these ions are presumably carried downstream and out of the specimen, causing resistivity to rise. Larger resistivity changes have been observed at the beginning of an experiment, when fluid first makes contact with the fracture surface, than after an extended period of flow. A drop in normalized resistivity for specimen DP3972.1 prior to flow was roughly twice that observed after extensive flow (Figure 7). Resistivity observations are discussed in greater detail in Carlson *et al.* (2004).

Figure 7. Resistivity during no-flow intervals

Flow Modeling

Flow simulations through the measured aperture fields provide estimates of local fluxes within the fractures before and after experiments. A finite-difference discretization of the local cubic law (e.g., Nicholl *et al*., 1999) is used to calculate the pressure field within the fractures and the corresponding local fluxes (Figure 8). The influence of aperture variability on local flow rates is clearly evident, and it is likely that these variations in local fluxes will lead to variability in local reaction rates within the fracture. Ongoing efforts are focused on coupling hydraulic and geochemical modeling to estimate variability in local reaction rates resulting from the combined influence of transport of reactants and products and local reaction kinetics.

Figure. 8. Flow simulations of fluid flux

Conclusions

Flow experiments at geothermal pressures and temperatures in artificially fractured specimens of Desert Peak quartz monzonite have shown reductions in permeability over time for two different injection fluids: one with and one without silica. Electrical resistivity measurements, which are sensitive to the ionic content of pore fluids, provide indirect evidence of geochemical activity. A contact surface profilometer has been used to characterize fracture surfaces prior to flow in two specimens. The profilometry data demonstrate that it is possible to fabricate statistically similar fracture surfaces and allow us to map fracture aperture variations. We use the aperture information to simulate flow. The flow simulations, when coupled to geochemical modeling, may lead to a better understanding of local variability in reaction rates.

Acknowledgements

Christy Morris and Ann Robertson-Tait provided the core and mineralogical analysis. David Ruddle prepared the samples. William Ralph provided technical assistance with the pressure system. Hansel Neurath provided software and data acquisition support. Bill Bourcier provided geochemistry advice, and Mackenzie Johnson helped with fluid preparation. The cooperation of ORMAT and GeothermEx is gratefully acknowledged.

This work was supported by the Office of Geothermal and Wind Technology under the Assistant Secretary for Energy Efficiency and Renewable Energy of the U.S. Department of Energy and the Office of Basic Energy Science. This work was performed under the auspices of the U.S. Department of Energy by University of California, Lawrence Livermore National Laboratory under Contract W-7405-Eng-48.

References

Azaroul, M., and C. Fouillac, 1997. "Experimental Study and Modeling of Granite-Distilled Water Interactions at 180°C and 14 Bars." *Applied Geochemistry*, v. 12, p. 55-73.

Carlson, S. R., J. J. Roberts, R. L. Detwiler, E. A. Burton, A. Robertson-Tait, C. Morris, and P. Kasameyer, 2004. "Fracture Permeability Evolution in Rock from the Desert Peak EGS Site." Geothermal Resources Council *Transactions*, v. 28, p. 279-284.

Chigira, M., and M. Watanabe, 1994. "Silica Precipitation Behavior in a Flow Field with Negative Temperature Gradients." *Journal of Geophysical Research*, v. 99, p. 15,539-15,548.

Durham, W. B., and B. P. Bonner, 1993. "PEAK: A New Kind of Surface Microscope." *International Journal of Rock Mechanics Mining Science and Geomechanical Abstracts*, v. 30, p. 699-702.

Lutz, S. J., 2003. "Summary of X-ray Diffraction Analysis." Energy & Geoscience Institute, University of Utah, 2 pp.

Lutz, S. J., A. Schriener, Jr., D. Schochet, and A. Robertson-Tait, 2003. "Geologic Characterization of Pre-Tertiary Rocks at the Desert Peak East EGS Project Site, Churchill County, Nevada." Geothermal Resources Council *Transactions*, v. 27, p. 865-870.

Moore, D. E., C. A. Morrow, and J. D. Byerlee, 1983."Chemical Reactions Accompanying Fluid Flow Through Granite Held in a Temperature Gradient." *Geochimica et Cosmochimica Acta*, v. 47, p. 445-453.

Moore, D. E., D. A. Lockner, and J. D. Byerlee, 1994. "Reduction of Permeability in Granite at Elevated Temperatures." *Science*, v. 265, p. 1558-1561.

Morrow, C. A., D. E. Moore, and D. A. Lockner, 2001. "Permeability Reduction in Granite under Hydrothermal Conditions." *Journal of Geophysical Research*, v. 106, p. 30,551-30,560.

Nicholl, M.J., H. Rajaram, R. J. Glass, and R. L. Detwiler, 1999. "Saturated Flow in a Single Fracture: Evaluation of the Reynolds Equations in Measured Aperture Fields." *Water Resources Research*, v. 35, p. 3361-3373.

Plagnes, V., I. Matsunaga, M. Azaroual, H. Tao, and K. Fujimoto, 2000. "Granite-Saline Fluid Interactions in a Dynamic Experimental System at 200°C and 50 Bars." *Proceedings, World Geothermal Conference 2000, Kyushu-Tohoku, Japan May 28 – June 10, 2000*, p. 3829-3834.

Polak, A., D. Elsworth, H. Yasuhara, A. S. Grader, and P. M. Halleck, 2003. "Permeability Reduction of a Natural Fracture under Net Dissolution by Hydrothermal Fluids." *Geophysical Research Letters*, v. 30, p. 2020-2024.

Robertson-Tait, A., and C. Morris, 2003. "Progress and Future Plans at the Desert Peak East EGS Project." Geothermal Resources Council *Transactions*, v. 27, p. 871-877.

Savage, D., K. Bateman, and H. G. Richards, 1992. "Granite-Water Interactions in a Flow-Through Experimental System with Applications to the Hot Dry Rock Geothermal System at Rosemanowes, Cornwall, U.K." *Applied Geochemistry*, v. 7, p. 223-241.

Viani, B. E., J. J. Roberts, R. L. Detwiler, S. K. Roberts, and S. R. Carlson, 2005. "Simulating Injectate/Rock Chemical Interaction in Fractured Desert Peak Quartz Monzonite." Geothermal Resources Council *Transactions,* v. 29.

Yasuhara, H., and D. Elsworth, 2004. "Evolution of Permeability in a Natural Fracture: Significant Role of Pressure Solution." *Journal of Geophysical Research*, v.109, B03204.

Table 1. Influent Chemical Composition, pH and Electrical Conductivity

	Saline Solution	Silica Solution
Na (mg/L)	3344	2942
K (mg/L)	0.0	349
Ca (mg/L)	0.0	150
SiO2 (mg/L)	0.0	58
Cl (mg/L)	5156	5118
Total Dissolved Solids (mg/L)	8500	8617
pH	6	7.4
Conductivity (mS/cm)	13.75	13.5

Table 2. Experimental Variables

Sample	Effect. Pressure (MPa)	Temp. (ºC)	Fluid Type	Flow Volume (L)	Test Length (days)	Flow Regime (days)			
						0.02 ml/min	0.01 ml/min	5.0 µl/min	No Flow
DP 3972.1	3.4	169	saline	2.1	111	64	11	16	20
DP 3972.2	3.4	167	saline	0.8	39	28	0	0	11
DP 3972.3	3.4	167	saline	NA	72	few	0	0	most
DP 3972.4	3.8	169	silica	1.0	37	37	0	0	0

Table 3. Effective Hydraulic Aperture from Variable Flow Rate Tests

Specimen	Day	Maximum Flow Rate (ml/min)	Regression Slope ($x10^{15}$)	Reynolds Number	Hydraulic Aperture (µm)	Error[1] (µm)
DP 3792.1	5	0.9	32.75	2.9	14.2	0.11
DP 3792.1	32	0.4	8.22	1.3	9.0[2]	0.08
DP 3792.1	67	0.12	1.24	0.38	4.8[2]	0.28
DP 3792.2	32	1.0	59.0	3.2	17.3	0.23
DP 3792.2	39	0.2	72.75	0.64	18.6	0.17
DP 3972.3	1	1.0	347.9	3.2	32.9	0.47
DP 3972.3	18	2.0	307.1	6.4	31.5	0.54
DP 3972.3	65	2.0	174.6	6.4	26.1	0.22
DP 3972.4	1	2.0	460.6	6.4	36.1	0.34
DP 3972.4	28	0.2	5.67	0.64	8.3	0.07

[1]Calculated from the standard error of the linear regression slope.
[2]A jacket leak may have affected the data.

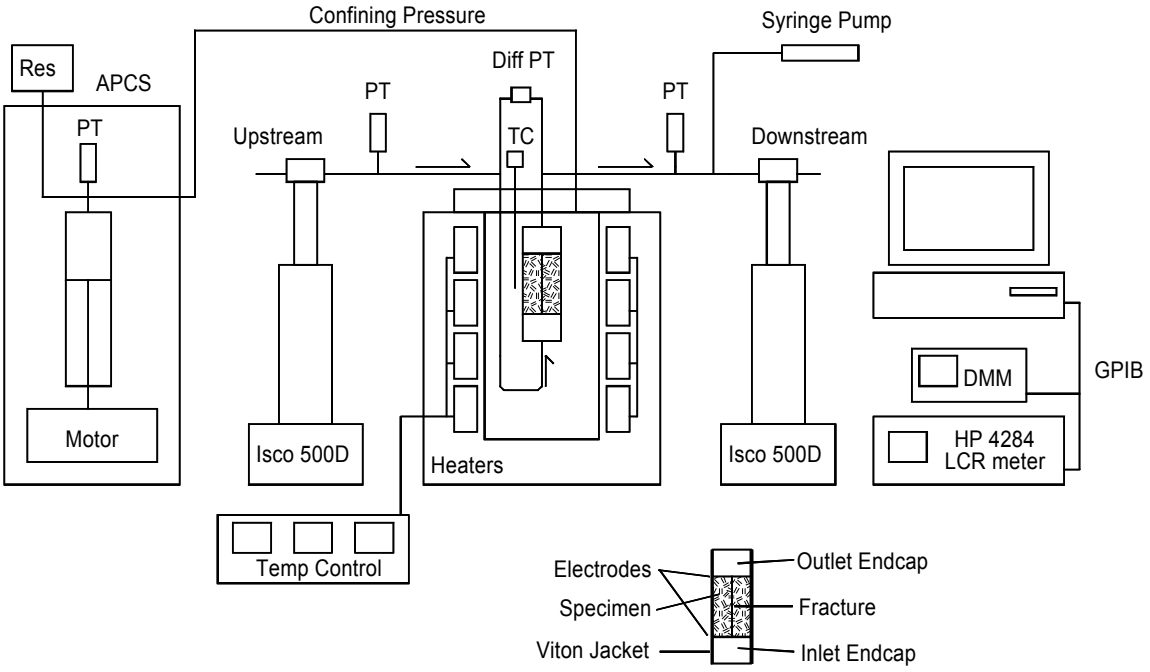

Fig. 1. Schematic diagram of the experimental apparatus and specimen assembly. The small syringe pump on the downstream line allows effluent samples to be collected without loss of pore pressure.

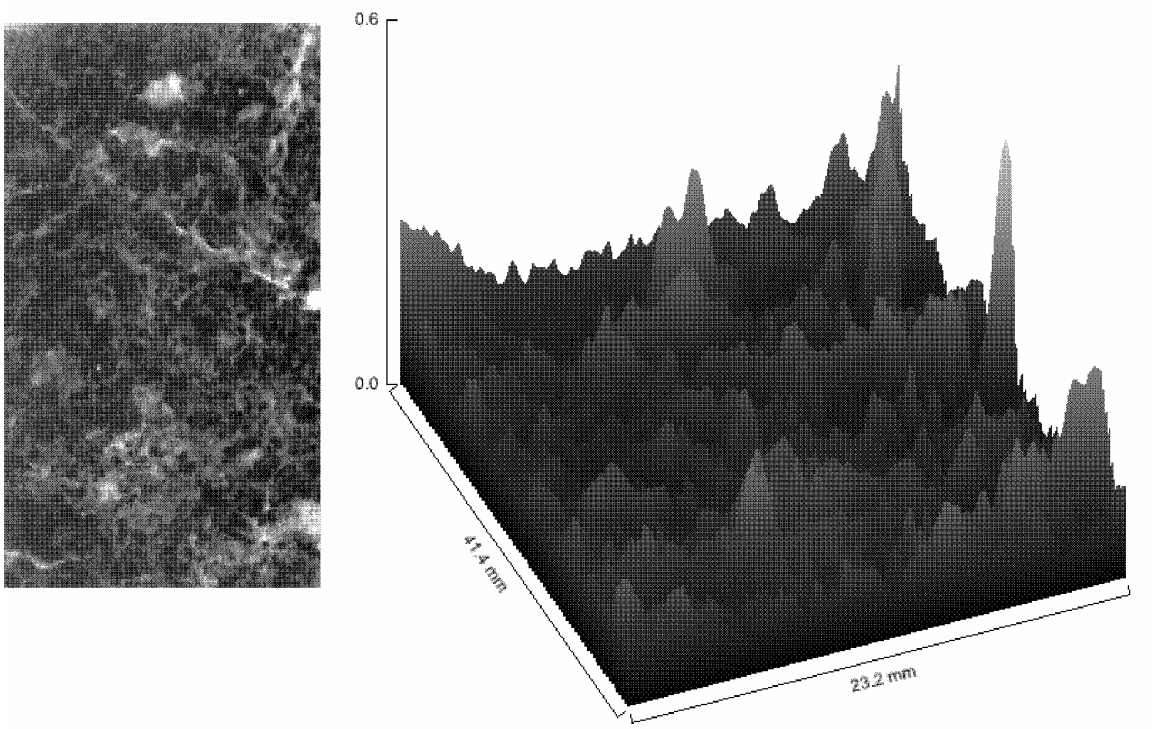

(a) (b)

Fig. 2. a) The bead-blasted surface of specimen DP 3972.4 from high-resolution surface profilometry. Scale: 0.0 mm (black) to -0.25 mm (white). b) Fracture apertures for specimen DP 3972.4. The vertical exaggeration is about 30x. The flow direction is from top to bottom for both images.

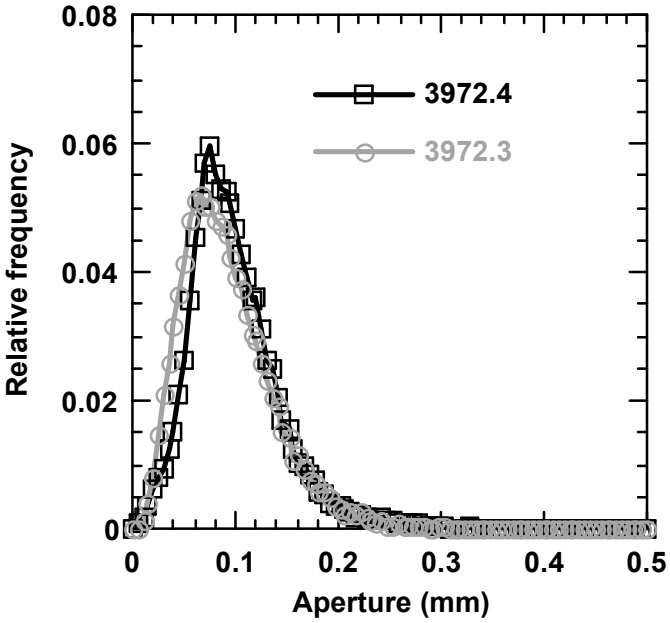

(a)

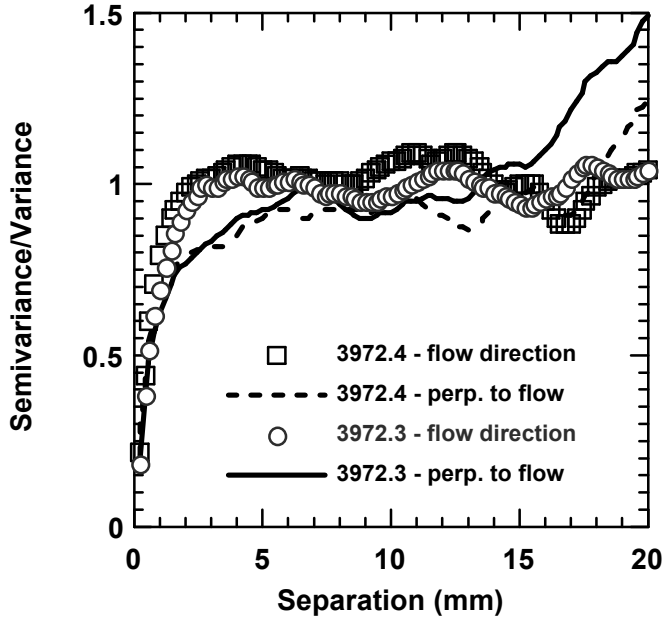

(b)

Fig. 3. a) Aperture frequency distributions for specimens DP 3972.3 and DP 3972.4, and b) Aperture semi-variograms measured parallel and perpendicular to the flow direction.

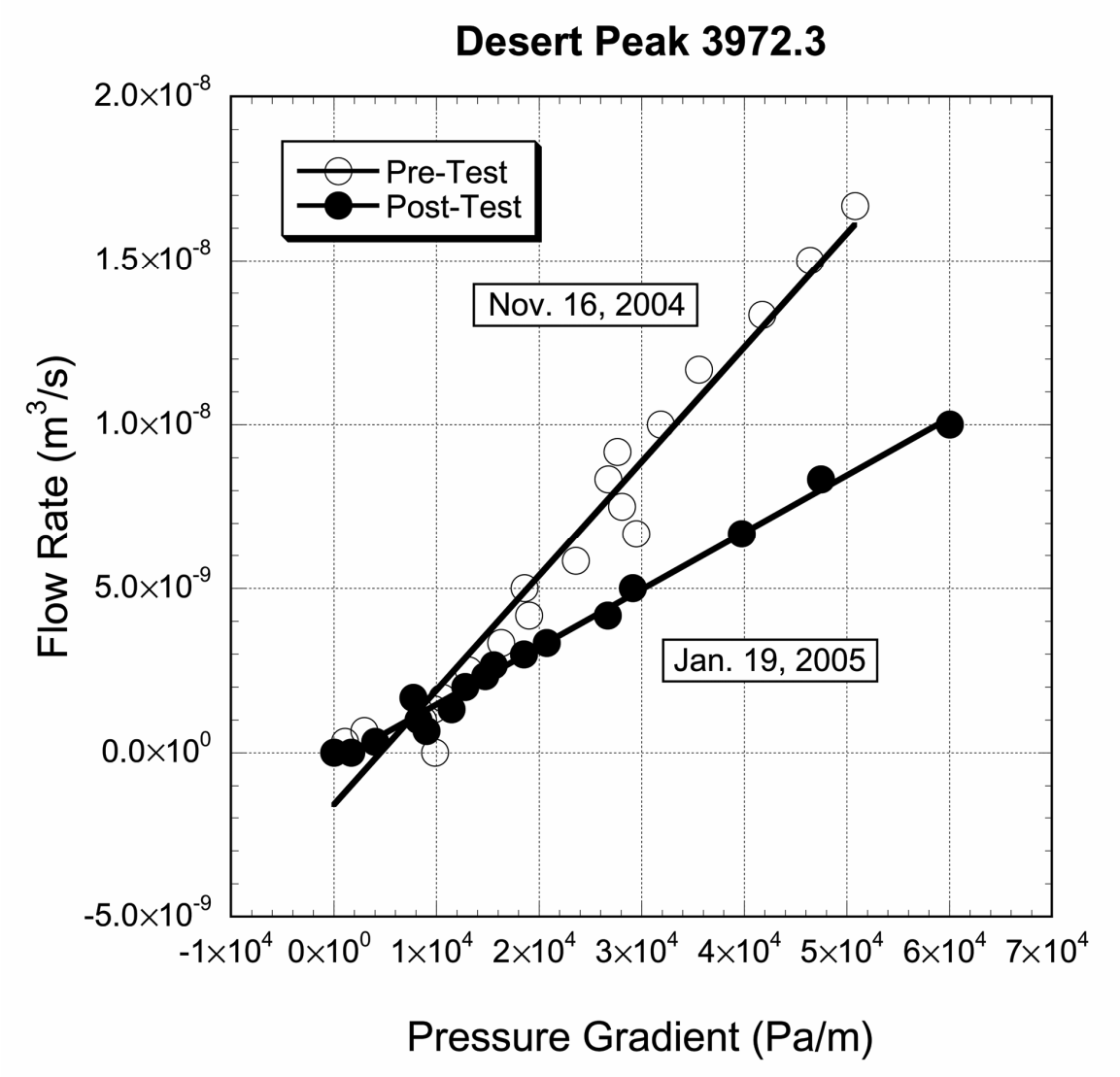

Fig. 4. Volumetric flow rate versus pore pressure gradient for specimen DP 3972.3 prior to flow (Pre-Test) and after a series of rapid flow tests (Post-Test). The slopes of the fitted lines are proportional to effective hydraulic aperture.

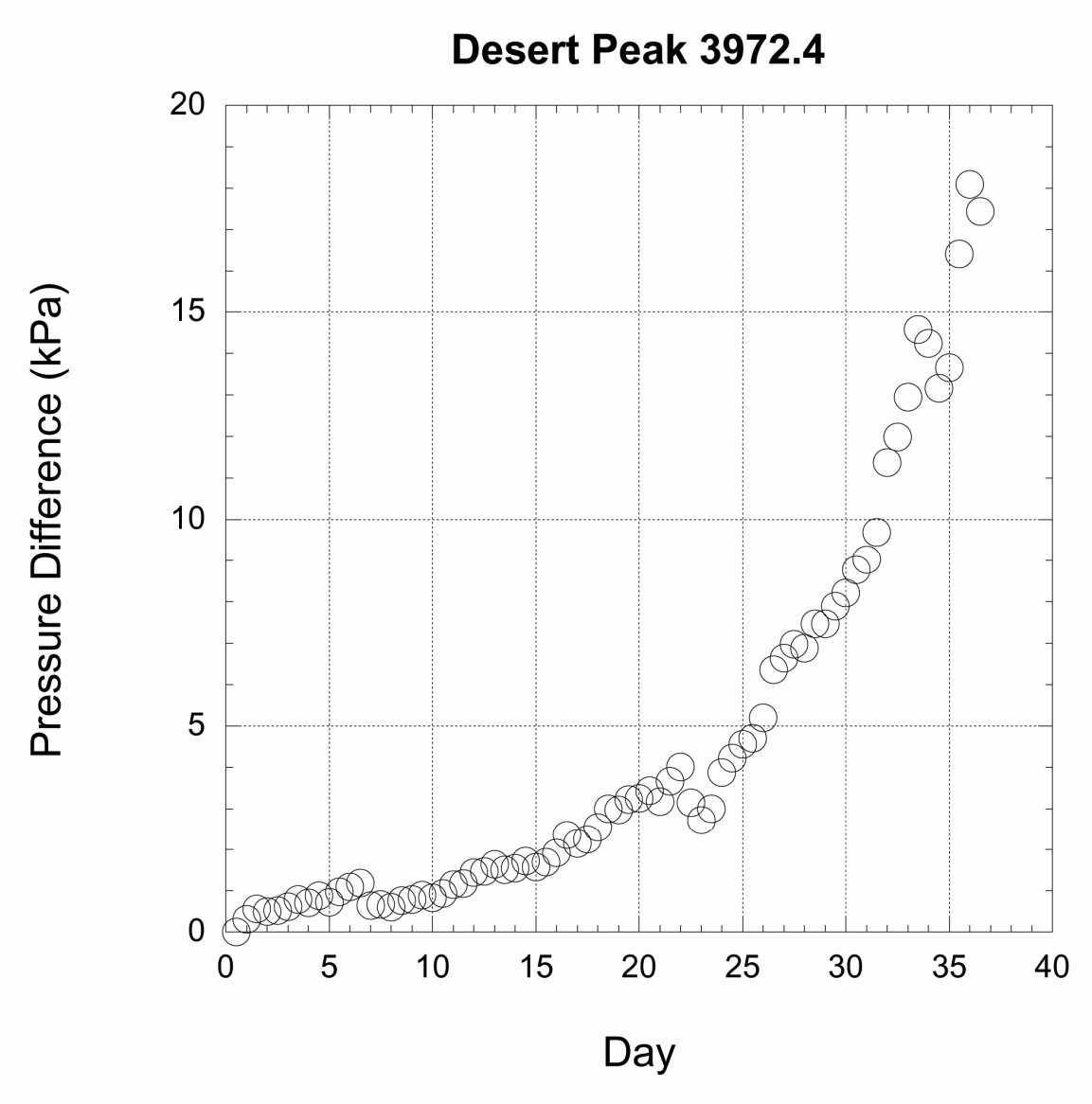

Fig. 5. Differential pressure (upstream minus downstream) at a constant flow rate of 0.02 mL/min for specimen DP 3972.4. Data are averaged over 12-hour intervals.

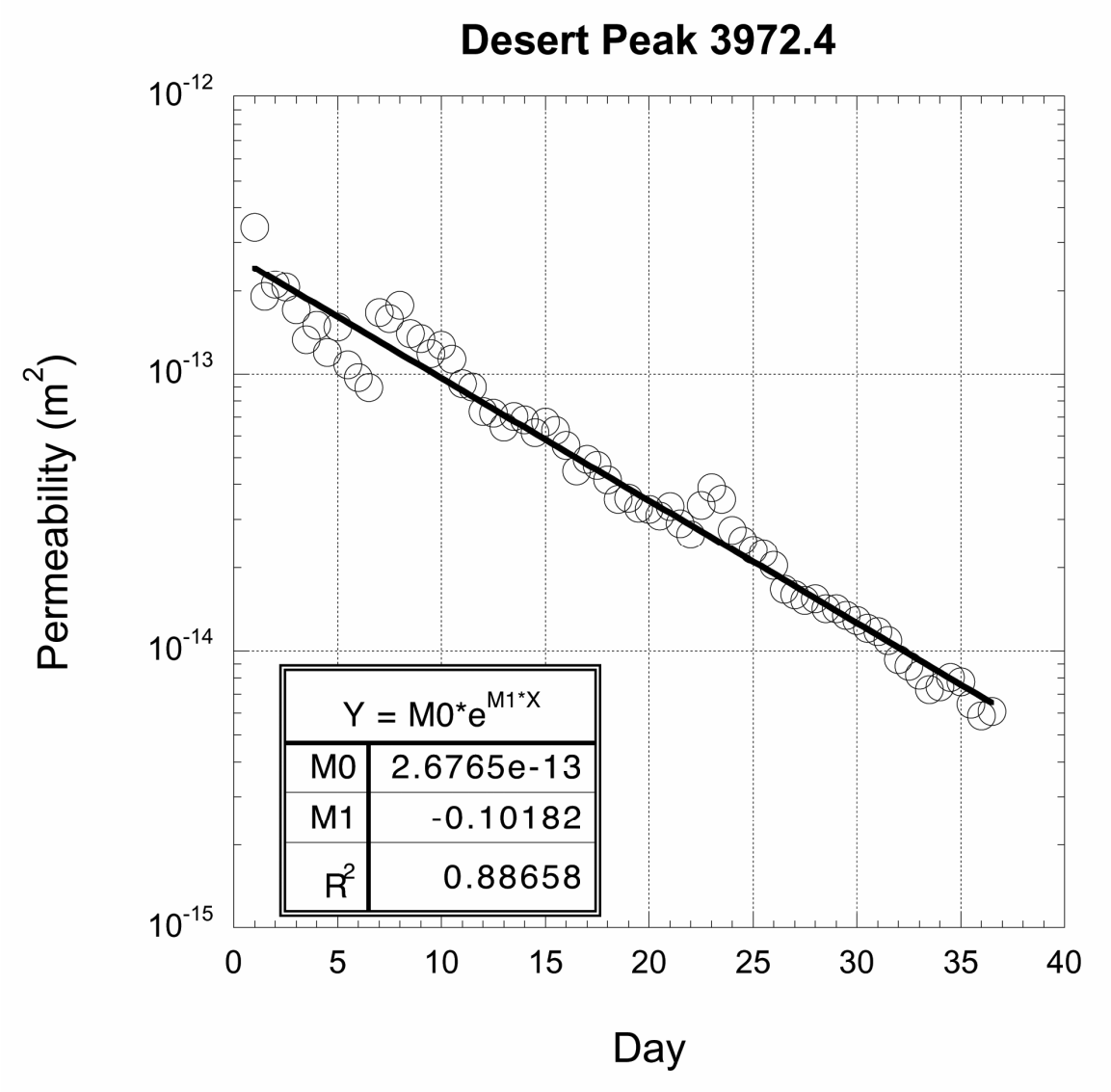

Fig. 6. Permeability for specimen DP 3972.4 over time, calculated from the differential pressure data of Figure 5.

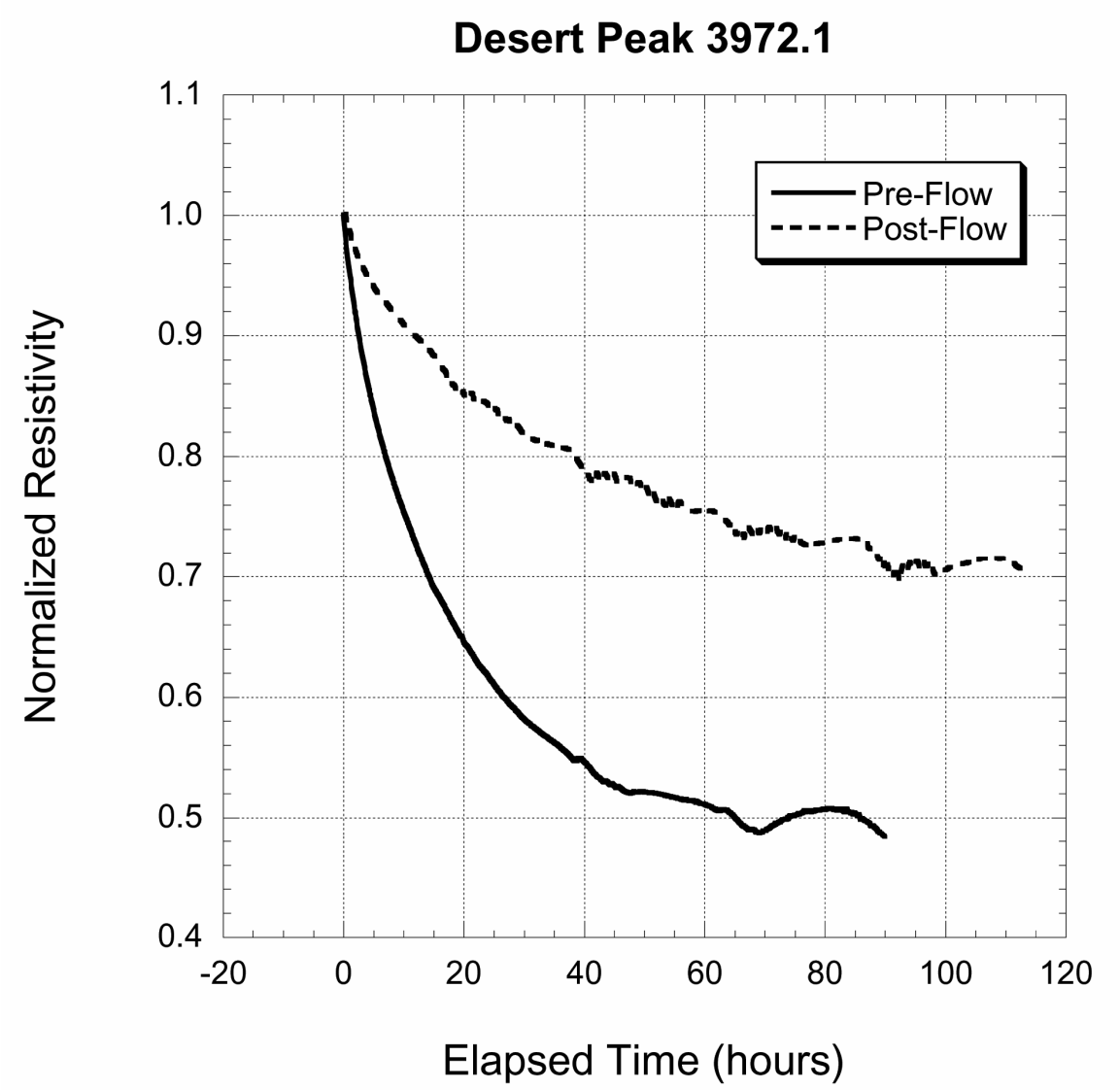

Fig. 7. Normalized electrical resistivity for specimen DP 3972.1 during intervals of no fluid flow. Pore fluid was in contact with relatively fresh fracture surfaces during Pre-Flow interval at the beginning of the experiment and with relatively weathered surfaces in the Post-Flow interval at the end of the experiment

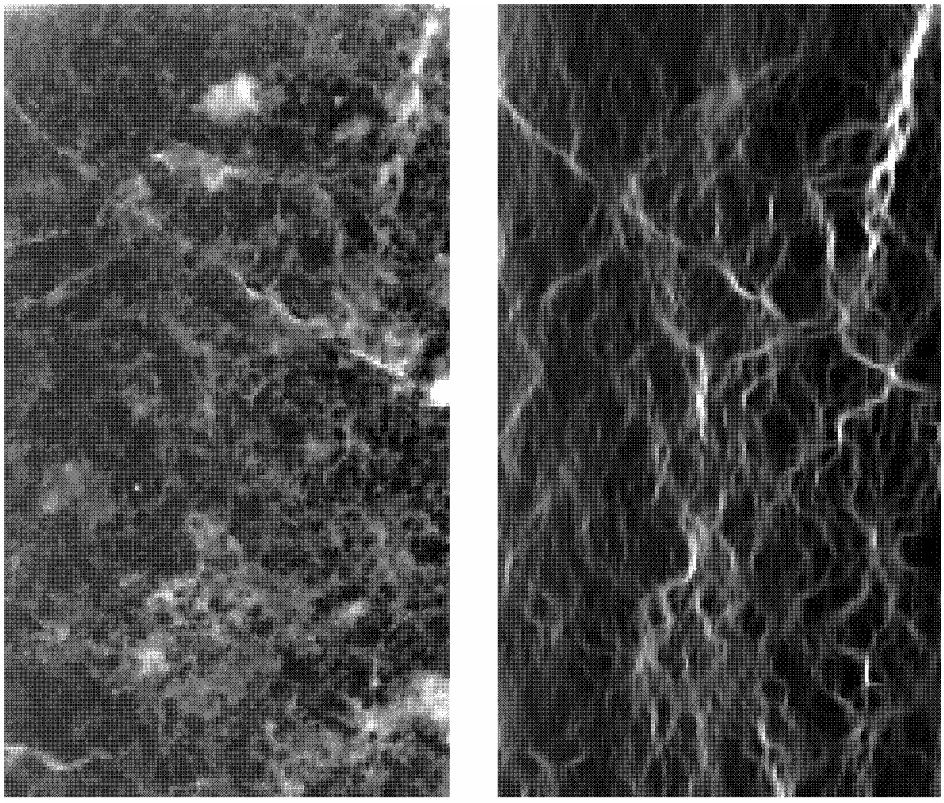

(a) (b)

Fig. 8. a) The bead-blasted fracture surface of specimen DP 3972.4 from profilometry data. Scale: 0.0 mm (black) to -0.25 mm (white). b) Fluxes from flow simulations for the same surface. Black represents low fluid flux; white high flux. The fluid flow direction is from top to bottom.